Os^{16+} and Ir^{17+} ions as candidates for accurate optical clocks sensitive to physics beyond the standard model

V. A. Dzuba and V. V. Flambaum
School of Physics, University of New South Wales, Sydney 2052, Australia

(Received 14 September 2023; accepted 30 October 2023; published 13 November 2023)

We perform detailed calculations of the electronic structure of the Os^{16+} ion and demonstrate that it has several metastable states which can be used for very accurate optical clocks. The clocks are highly sensitive to manifestations of the physics beyond the standard model, such as time variation of the fine-structure constant α, interaction with scalar and pseudoscalar (axion) dark matter fields, local Lorentz invariance and local position invariance violations, and interaction of atomic electrons with a nucleus mediated by a new boson. The latter can be studied by analyzing the King plot for isotope shifts and its possible nonlinearities since Os has five stable isotopes with zero nuclear spin. Similar calculations for the Ir^{17+} ion spectra demonstrate good agreement between theory and experiment. This helps to validate the method of the calculations and demonstrate that both ions are excellent candidates for the search for new physics.

DOI: 10.1103/PhysRevA.108.053111

I. INTRODUCTION

It was suggested in Refs. [1] to use highly charged ions (HCIs) to search for optical transitions highly sensitive to the time variation of the fine-structure constant α. The idea is based on the fact of the *level crossing* [2]. Usually intervals between electron energy levels are very large in HCIs compared to neutral atoms. However, due to different level ordering in neutral atoms and hydrogenlike ions, the energy interval between states of different configurations, drawn as a function of the ionization degree Z_i, must cross at some point, bringing the energy interval into the optical region. Since states of different configurations have different dependencies on the value of the fine-structure constant α, the energy intervals are very sensitive to the variation of α. The sensitivity is proportional to $Z^2(Z_i+1)^2$ and strongly depends on the electron orbital angular momentum. The largest sensitivity can be found in electron transitions in heavy ions which in the single-electron approximation can be described as $s_{1/2}$-$f_{5/2}$, $f_{7/2}$ or $p_{1/2}$-$f_{5/2}$, $f_{7/2}$ (s-f or p-f) transitions [1–3]. Use of metastable states brings the additional advantage of potentially very high accuracy of the measurements typical for atomic optical clocks. The accuracy for HCI clocks can be even higher than that for optical clocks in neural atoms due to the fact that states of HCIs are less sensitive to perturbations due to the compact size of HCIs, small polarizability, and large energies of excitations [4].

A number of candidate systems were suggested in earlier works [4–7] (see also reviews [8,9] and references therein). Experimental studies were performed for Ho^{14+} [10,11] and Ir^{17+} [12] ions. Further work is in progress [8,9]. In the present work we study the Os^{16+} ion. It has some important features which make it an attractive candidate for experimental study. It has several metastable states which can be used for clock transitions. At least one transition is the s-f transition, so that it is very sensitive to the variation of the fine-structure constant α and the dark matter field which may be a source of such variation [13–15]. Other transitions are less sensitive to α variation and can serve as *anchor* lines. In addition, they are sensitive to other manifestations of new physics such as local Lorentz invariance and local position invariance violations, etc. The energy diagram for the Os^{16+} ion is presented in Fig. 1. This diagram is the result of the calculations in the present work. Experimental energy intervals between states of different configurations are not known,

The Os^{16+} ion is similar to the Ir^{17+} ion studied before [12,16]. However, it has the important advantage of having five stable isotopes with zero nuclear spin (Ir has none). It makes this ion suitable for searching for new interactions via looking at possible nonlinearities of the King plot [18,19]. The minimum requirements for such study include having two clock transitions and four stable isotopes. Isotopes with zero nuclear spin have the further advantage of having no hyperfine structure which complicates the analysis of the isotope shift. Table I lists five stable isotopes of Os, which have zero nuclear spin. It also presents the β parameters of nuclear quadrupole deformation. These parameters come from nuclear calculations [17]. Nuclear deformation can lead to the nonlinearities of the King plot [20,21], presenting an important systematic effect in the search for new interactions. Note, however, that the parameters of deformation have similar values for all stable isotopes (see Table I). This means that significant cancellation of the effect of deformation is possible in the isotope shift.

Finally, the Os^{16+} and Ir^{17+} ions are suitable for searching the effects of local Lorentz invariance (LLI) and local position invariance (LPI) violation, since these effects are strongly enhanced in HCIs [22]. It was argued in Refs. [22,23] that to have an enhanced value of the LLI violation one needs to have a long-living state (e.g., ground) with a large value of the total electron momentum J ($J \geqslant 2$) and large values of the matrix element for the LLI violating operator. Such states can often be found in open $4f$ shells. All these conditions are satisfied

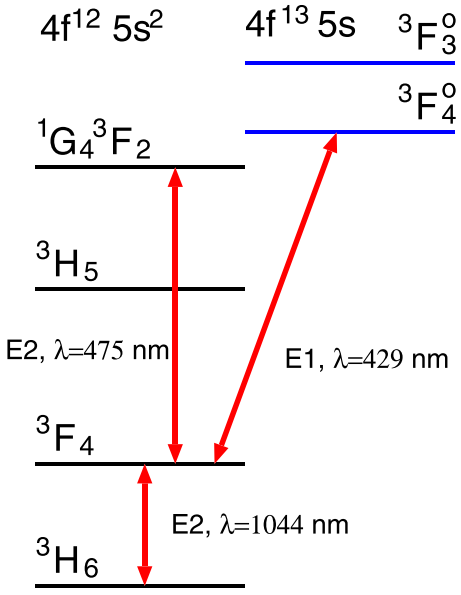

FIG. 1. Energy level diagram for the Os^{16+} ion. Possible clock transitions within the even configuration and the s-f transition are shown as red double arrows.

for metastable states of the Os^{16+} and Ir^{17+} ions, including the ground state. The situation with the LPI violating effect in HCIs is similar to that of the LLI violating effect.

II. METHOD OF CALCULATIONS

The Os^{16+} ion has an open $4f$ shell. Its ground-state configuration is $[Pd]4f^{12}5s^2$, while we study also the states of the $[Pd]4f^{13}5s$ configuration. The ion has 14 electrons in open shells. This number is too large for standard configuration interaction (CI) calculations. In the present work, we use the configuration interaction with perturbation theory (CIPT) method [24] especially developed for such systems. The method was used for many atoms and ions with open d or f shells (see, e.g., Refs. [25–27]) and it has been proven to be very useful. The best results are achieved for systems with almost empty or almost full open shells. On the other hand, the systems with half-filled d or f shells are the most difficult for calculations. Since the accuracy for different systems is different, it is always useful to do some additional tests for similar systems where experimental data or other calculations are available. In this work we study the Os^{16+} and Ir^{17+} ions. Both ions have similar electronic structure (the configurations are the same but the states go in different order). There are experimental data on a number of transition energies for both ions [12]. The same paper also presents several different calculations. However, the data on the Ir^{17+} ion is more complete. Experimental data include energies for some $E1$ transitions between states of different configurations, while the data for Os^{16+} contains only energies of $M1$ transitions between states of the same configuration. The $E1$ transitions present a special interest because of their sensitivity to the variation of the fine-structure constant. The initial idea of using the Ir^{17+} ion comes from the finding that the energy of the $E1$ transition is in the optical region [5]. Very advanced calculations by a different method [16] are also available for Ir^{17+}. Therefore, we use calculations for Ir^{17+} to check the accuracy and applicability of the CIPT method to the Os^{16+} ion.

TABLE I. A list of stable isotopes of Os with zero nuclear spin. The β parameters of the quadrupole deformation of proton distribution are taken from Ref. [17].

A	184	186	188	190	192
β	0.281	0.257	0.223	0.185	0.164

A. Calculation of energies

The wave function for 14 external electrons of the Os^{16+} ion in the CIPT method is presented as an expansion over single-determinant many-electron basis functions:

$$\Psi(r_1,\ldots,r_{N_e}) = \sum_{i=1}^{N_1} c_i\Phi_i(r_1,\ldots,r_{N_e}) + \sum_{i=N_1+1}^{N_2} c_i\Phi_i(r_1,\ldots,r_{N_e}). \quad (1)$$

Here N_e is the number of external electrons ($N_e = 14$ in our case). The expansion is divided into two parts. It is assumed that first few low-energy (the energy is related to the basis state by $E_i = \langle\Phi_i|\hat{H}^{\rm CI}|\Phi_i\rangle$) terms present good approximation for the wave function, while the huge number ($N_2 \gg N_1$) of remaining high-energy terms is just a small correction. Calculations start from the relativistic Hartree-Fock (RHF) method applied to the open-shell ion. To make sure that the first part of expansion (1) presents a good approximation for the wave function, the electron configuration in the RHF calculations should coincide with one of the configurations of interest. In our case, these are the $4f^{12}5s^2$ and $4f^{13}5s$ configurations. Changing the initial choice from one configuration to another changes the energy intervals between states of different configurations by a few thousand cm^{-1} without changing the order of the states. We have chosen the $4f^{13}5s$ configuration in the RHF because this gives good results for Ir^{17+} (see the next section). The RHF Hamiltonian has the form

$$\hat{H}^{\rm RHF} = c\alpha\cdot\mathbf{p} + (\beta-1)mc^2 + V_{\rm nuc} + V_{\rm Breit} + V_{\rm QED} + V_e, \quad (2)$$

where c is speed of light, α and β are Dirac matrices, $\mathbf{p}$ is the electron momentum, $V_{\rm nuc}$ is the nuclear potential obtained by integrating the Fermi distribution of the nuclear charge, $V_{\rm Breit}$ is the operator of the Breit interaction which includes magnetic interaction and retardation [28] in a zero-frequency approximation (see, e.g., Ref. [29]), $V_{\rm QED}$ is the potential which simulates quantum electrodynamic corrections [30], and V_e is the electron self-consistent RHF potential with contributions from all 60 electrons of the Os^{16+} ion including the electrons of the $4f^{13}5s$ configuration. At the next stage the single-electron basis is calculated in the field of the frozen core using the B-spline technique [31].

Then, applying the standard CI technique and neglecting the off-diagonal matrix elements between high-energy states,

TABLE II. Parameters of the CIPT calculations for the Os^{16+} ion. J^p stands for the total angular momentum and parity. One even configuration ($4f^{12}5s^2$) and two odd configurations ($4f^{13}5s$ and $4f^{12}5s5p$) are used to generate states in the effective CI matrix. The second odd configuration is added to allow electric dipole transitions between states of even and odd configurations (see Fig. 2). N_c is the corresponding number of relativistic configurations; N_1 is the corresponding number of states with given J^p; $N_1 \times N_1$ is the size of the effective CI matrix; and N_2 is the number of terms in the second-order correction [second term in Eq. (3)].

J^p	N_c	N_1	N_2
3^-	8	26	$\sim 3 \times 10^5$
4^-	7	24	$\sim 3 \times 10^5$
2^+	3	3	$\sim 6 \times 10^6$
3^+	3	1	$\sim 1.5 \times 10^7$
4^+	3	3	$\sim 4 \times 10^6$
5^+	3	1	$\sim 1.0 \times 10^7$
6^+	3	2	$\sim 4 \times 10^6$

one gets the CIPT equation

$$\left[\langle i|\hat{H}^{\rm CI}|j\rangle + \sum_m^{N_2} \frac{\langle i|\hat{H}^{\rm CI}|m\rangle\langle m|\hat{H}^{\rm CI}|j\rangle}{E - E_m}\right]\mathbf{X} = E\mathbf{X}. \quad (3)$$

Here $\mathbf{X}$ is the vector of unknown expansion coefficients, $\mathbf{X} = (c_1, \ldots, c_{N_1})$. Indexes i, j, and m numerate many-electron basis states $|\Phi\rangle$, indexes i and j run from 1 to N_1, and index m runs from $N_1 + 1$ to N_2. Operator $\hat{H}^{\rm CI}$ is the CI Hamiltonian

$$\hat{H}^{\rm CI} = \sum_{i=1}^{N_e} \hat{H}_{1i} + \sum_{i>j}^{N_e} \frac{e^2}{|\mathbf{r}_i - \mathbf{r}_j|}, \quad (4)$$

where $\hat{H}_{1i}$ is the single-electron part of the Hamiltonian similar to Eq. (2) but with V_e replaced by $V_{\rm core}$. Only core electrons (up to the $4d$ shell) contribute the the $V_{\rm core}$ potential, while all ionic electrons (including the $4f^{13}5s$ configuration) contribute the V_e potential. We do not include $V_{\rm Breit}$ in the CI Hamiltonian because the Breit interaction between valence electrons is a small correction which is much smaller than the uncertainty coming from other sources. The inclusion of Breit and QED corrections is important in the RHF stage only since it involves all atomic electrons including innershell relativistic electrons.

The typical values of the N_1 and N_2 parameters for different states of Os^{16+} are presented in Table II. The value of N_1 is the size of the effective CI matrix. Note that it is always small. The main challenge of the method is the calculation of the second-order correction containing the huge number of terms ($N_1 \times N_2$, see Table II for the values).

The energy E in Eq. (3) is the energy of the state to be found from solving the CIPT equations. It presents in both left- and right-hand sides of the equation. This means that iterations are needed to solve the equations. Iterations can start from solving the CIPT equations (3) without the second-order correction. In most cases less than ten iterations are sufficient for full convergence.

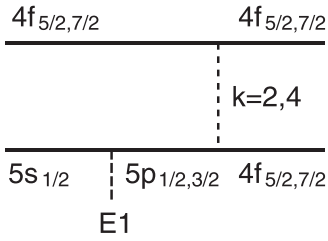

FIG. 2. Dominating contributions to the electric dipole ($E1$) transition between states of even ($4f^{12}5s^2$) and odd ($4f^{13}5s$) configurations. The transition is due to the mixing of the odd states of the $4f^{13}5s$ and $4f^{12}5s5p$ configurations.

B. Calculation of matrix elements

To calculate matrix elements of transitions between states and energy shifts due to different effects which were not included in the calculations of energy, we use the time-dependent Hartree-Fock (TDHF) method [32] which is equivalent to the well-known random-phase approximation (RPA). The RPA equations have the form

$$(\hat{H}^{\rm RHF} - \epsilon_c)\delta\psi_c = -\left(\hat{F} + \delta V_e^F\right)\psi_c. \quad (5)$$

Here $\hat{H}^{\rm RHF}$ is given by Eq. (2), index c numerates the single-electron states of the ion (the same as in the RHF calculations), $\hat{F}$ is the operator of external field, $\delta\psi_c$ is the correction to the wave function due to the external field, and δV_e^F is the correction to the self-consistent RHF potential caused by the change of all ionic states.

The RPA equations are solved self-consistently for all RHF states of the ion. Then the transition amplitude is given by

$$T_{ij} = \langle\Psi_i| \sum_{m=1}^{N_e} \left(\hat{F} + \delta V_e^F\right)_m |\Psi_j\rangle, \quad (6)$$

where $|\Psi_i\rangle$ and $|\Psi_j\rangle$ come from solving the CIPT equations (3). For energy shifts, $i = j$ in Eq. (6).

Note that in some cases one needs to include more terms in the first part of the wave function expansion (1) to allow for nonzero values of the transition amplitudes. For example, the electric dipole ($E1$) transition cannot go directly between states of the $4f^{13}5s$ and $4f^{12}5s^2$ configurations because in this case it would correspond to the s-f single-electron transition which is forbidden by the selection rules. One needs to add at least the $4f^{12}5s5p$ configuration to mix with the $4f^{13}5s$ configuration. Then the $E1$ transition amplitude is given by Fig. 2.

C. Energy levels of Ir^{17+}: Discussion of accuracy

The Ir^{17+} ion was proposed for the measurements in Ref. [5] and studied both experimentally and theoretically (see Refs. [12,16] and references therein). It is very similar to the Os^{16+} ion studied in the present work. It has the same number of external electrons forming the same configurations and many other similarities. It is natural to expect that the accuracy of the calculations for both ions is very similar too. Therefore, we perform exactly the same calculations for both ions and compare our results with experiment and previous calculations. Our first calculations for the Ir^{17+} ion [5] used a

TABLE III. Energy levels and g factors of the Ir^{17+} ion. Comparison with previous calculations and experiment. Experimental energies are obtained from measured transition energies [12]; see also Tables IV and V.

		Energies (cm^{-1})			g factors	
Configuration	Term	Ref. [5]	Ref. [16]	Expt.	Present work	
			Odd states			
$4f^{13}5s$	$^3F^o_4$	0	0		0	1.2500
	$^3F^o_3$	4838	4777		4647	1.0515
	$^3F^o_2$	26272	25186		25198	0.6667
	$^1F^o_3$	31492	30395	30359	30167	1.0318
			Even states			
$4f^{14}$	$^1S_0$	5055	12382		7424	0.0000
$4f^{12}5s^2$	$^3H_6$	35285	30283		29695	1.1641
	$^3F_4$	45214	39564	41639	39563	1.1377
	$^3H_5$	59727	53798		53668	1.0333
	$^3F_2$	68538	61429	62930	62140	0.8331
	$^1G_4$	68885	62261	64588	62380	0.9902
	$^3F_3$	71917	65180	67154	65438	1.0833
	$^3H_4$	92224	84524		84662	0.9221
	$^1D_2$	98067	89273	90317	91341	1.1315
	$^1J_6$	110065	101136		103487	1.0026

different method which was less accurate, especially for the energy intervals between states of different configurations. It had fitting parameters which would allow one to fix the interval when the experimental value is known. However, in the absence of the experimental data the predictions were not very accurate. In contrast, our present method is fully *ab initio* and produces more accurate results. There were many other calculations (see Ref. [12] and references therein). The most sophisticated and accurate calculations were reported in Ref. [16]. The agreement with experiment was very good. Therefore, we compare our present results only with experiment and calculations of Ref. [16].

Energy levels of the Ir^{17+} ion are presented in Table III, $M1$ transition energies are presented in Table IV, and $E1$ transition energies are presented in Table V. In all these tables, our results are compared with previous calculations and experiment. Note that experimental work [12] presents only transition energies which are not translated into energy levels. This is because the interpretation of the $E1$ transition energies was ambiguous. Table V gives two alternative interpretations given in Ref. [12]. Both calculations, present work and Ref. [16], support the first version. Using this interpretation of the experimental data allows one to reconstruct some experimental energy levels. The results are presented in Table III. Note good agreement between the latest calculations and between theory and experiment, while our old results [5] are less accurate. There is one state ($^3F_3$) for which the agreement between theory and experiment is poor. This leads to poor agreement for the transition energy involving this state (the $^1D_2$ - $^3F_3$ transition, see Table IV). It is interesting to note that both theoretical results for this state agree well with each other but not with experiment. It was noted in Ref. [16] that one possible reason for this might be the wrong interpretation of experimental data. However, we do not see any alternative interpretation. In the end, the reason for poor accuracy is not clear.

TABLE IV. $M1$ transition energies in the Ir^{17+} ion (in cm^{-1}). Comparison with previous calculations and experiment. $\Delta E/E$ is the relative deviation of our results from the experimental energies (in %).

			Expt.	Theory		
Configuration	Terms		Ref. [12]	Ref. [16]	Present	$\Delta E/E$
$4f^{13}5s$	$^3F^o_2$	– $^3F^o_3$	20711	20409	20551	−0.8
	$^1F^o_3$	– $^3F^o_4$	30359	30395	30168	−0.6
$4f^{12}5s^2$	$^3H_5$	– $^3H_6$	23640	23515	23973	1.4
	$^3H_4$	– $^1G_4$	22430	22263	22282	−0.7
	$^1G_4$	– $^3F_4$	22949	22697	22817	1.7
	$^1D_2$	– $^3F_3$	23163	24093	25903	12
	$^3F_3$	– $^3F_4$	25515	25616	25875	1.4
	$^1D_2$	– $^3F_2$	27387	27844	29201	6.6
	$^3H_4$	– $^3H_5$	30798	30726	30994	0.6

TABLE V. $E1$ transition energies in the Ir^{17+} ion (in cm^{-1}). Comparison with the previous calculations and experiment.

					Expt. [12]	
Terms			Ref. [16]	Present	Version 1	Version 2
$^3F_4$	–	$^3F^o_4$	39568	39563	41639	
$^3F_3$	–	$^1F^o_3$	34785	35271	36796	41639
$^1G_4$	–	$^1F^o_3$	31866	32213		39072

Another large deviation between theory and experiment is for the $^1D_2$ - $^3F_2$ transition (6.6%). Note, however, that the accuracy for each state is good, ∼1% (see Table III). But it is −1% for the lower state and +1% for the upper state. This leads to a larger relative deviation in the difference.

In the end, the agreement between theory and experiment is within 3% for all states and most energy intervals. We expect similar accuracy for the Os^{16+} ion.

III. CALCULATIONS FOR THE Os^{16+} ION: IDENTIFICATION OF THE CLOCK TRANSITIONS

We have calculated energies, g factors, lifetimes, and other characteristics of the low-lying states of Os^{16+}. The results are presented in Table VI. The list of states is very similar to that of the Ir^{17+} ion (see previous section), but the states go in a different order.

Lifetimes (τ) of even states are calculated by including all possible $M1$ and $E2$ transitions to low states. Lifetimes of odd states are calculated by taking into account $E1$ transitions to lower even states. We see at least two metastable states, the first excited state at $E = 9853\ cm^{-1}$ and $\tau = 1400$s, and the $^3F_2$ state at $E = 30\,675\ cm^{-1}$ and $\tau = 156$s. The first odd state at $E = 32\,908\ cm^{-1}$ is also relatively long-living, $\tau = 96$ ms. In principle, all these states can be used for high-precision measurements. Corresponding clock transitions within the even configuration and the s-f transition are shown in Fig. 1.

TABLE VI. Excitation energies (E), g factors, and other characteristics of low-lying states of the Os^{16+} ion. The numbers in the second column are experimental energies reconstructed from transition energies presented in the Supplemental Material of Ref. [12]. τ is the lifetime, α_0 and α_2 are the static scalar and tensor polarizabilities, and Q is the electric quadrupole moment.

	E (cm^-1)			τ	α_0	α_2	Q
Term	[12]	Present	g	s	a_0^3	a_0^3	a.u.
			Even states, $4f^{12}5s^2$				
$^3H_6$	0	0	1.164		0.5310	−0.0085	0.194
$^3F_4$	9049	9583	1.137	1.4[+4]	0.5307	0.0006	−0.018
$^3H_5$	21176	22433	1.033	4.0[−3]	0.5309	−0.0074	0.171
$^3F_2$	28951	30675	0.824	156	0.5304	0.0036	−0.087
$^1G_4$	29109	30643	0.989	10[−3]	0.5307	−0.0033	0.075
$^3F_3$	31931	33525	1.083	5.2[−3]	0.5305	0.0018	−0.047
$^3H_4$	49240	50086	0.927				
$^3F_2$	54221	58036	1.130				
			Odd states, $4f^{13}5s$				
$^3F_4^o$		32908	1.2500	96[−3]	0.0450	1.2[−5]	0.191
$^3F_3^o$		37432	1.0524	38[−3]	0.0450	8.4[−5]	0.161

The $E1$ amplitude $\langle {}^3\mathrm{F}_4^o||E1||{}^3\mathrm{F}_4\rangle = 1.91 \times 10^{-3} a_B$ is small due to the configuration mixing and the compact ion size. The values of the $E1$ transition amplitudes for Ir^{17+} are similar. For example, for three transitions presented in Table V, the values are $2.3 \times 10^{-3} a_B$, $7.6 \times 10^{-4} a_B$, and $3.1 \times 10^{-3} a_B$, respectively.

To find the effect of black-body radiation (BBR) on clock transitions we have calculated static dipole polarizabilities of the low states of Os^{16+}. The calculations were performed by a method especially developed in our earlier work [33] for atoms with open shells. The results are presented in Table VI (static tensor polarizabilities α_2 are also included). The BBR shift (in Hz) is given by (see, e.g., Ref. [34])

$$\delta\nu_{\mathrm{BBR}} = -8.611 \times 10^{-3} \left(\frac{T}{300\ \mathrm{K}}\right)^4 \Delta\alpha_0. \tag{7}$$

Using numbers from Table VI, one gets $\delta\nu/\nu \sim 10^{-20}$ for the $E2$ clock transitions and $\delta\nu/\nu \sim 10^{-17}$ for the s-f transition.

All clock states of the Os^{16+} ion have a relatively large total angular momentum J. This means that the states might be sensitive to the gradient of the electric field ε via quadrupole interaction. The corresponding energy shift is given by

$$\Delta E_Q = \frac{J_z^2 - J(J+1)}{2J(2J-1)} Q \frac{\partial \varepsilon_z}{\partial z}, \tag{8}$$

where Q is atomic quadrupole moment defined as the doubled expectation value of the $E2$ operator in the stretched state:

$$Q = 2\langle J, J_z = J|E2|J, J_z = J\rangle. \tag{9}$$

The calculated values of the quadrupole moment Q for low states of Os^{16+} are presented in Table VI.

IV. SEARCH FOR NEW PHYSICS

A. Time variation of the fine-structure constant

High sensitivity to the variation of the fine-structure constant α ($\alpha = e^2/\hbar c$) was the primary reason for suggesting the ions like Os^{16+}, Ir^{17+}, and others for the measurements [1,5]. The largest sensitivity corresponds to the largest change of the total electron angular momentum j in the single-electron approximation for atomic transition [1]. Both ions, Os^{16+} and Ir^{17+}, have optical transition between states of the $4f^{12}5s^2$ and $4f^{13}5s$ configurations, which correspond to the s-f single-electron transition ($\Delta j = 2$ or 3).

To find the sensitivity of atomic transitions to the variation of α, we write the frequencies of the transitions in the form

$$\omega_a(x) = \omega_{a0} + q_a x, \tag{10}$$

where $x = [(\alpha/\alpha_0)^2 - 1]$, α_0 is physical value of α, and q is the sensitivity coefficient to be found from calculations. To find q we vary the value of α in computer codes and calculate the numerical derivative

$$q_a = \frac{\omega_a(\delta) - \omega_a(-\delta)}{2\delta}. \tag{11}$$

Usually, we take $\delta = 0.01$. Varying δ is useful for checking the stability of the results.

To search the manifestation of the variation of the fine-structure constant, we need at least two atomic transitions and we measure one frequency against the other over a long period of time. Then the relative change of frequencies can be written as

$$\frac{\delta\omega_a}{\omega_a} - \frac{\delta\omega_b}{\omega_b} = \left(\frac{2q_a}{\omega_a} - \frac{2q_b}{\omega_b}\right)\frac{\delta\alpha}{\alpha} \equiv (K_a - K_b)\frac{\delta\alpha}{\alpha}, \tag{12}$$

where the dimensionless parameter K ($K = 2q/\omega$) is called the enhancement factor. It is obvious from Eq. (12) that for the highest sensitivity one needs two transitions with very different values of K; e.g., one is large and another is small or has the opposite sign. The calculated values of q and K are presented in Table VII. The results for Os^{16+} have been obtained in the present work while the results for Ir^{17+} are taken from Ref. [5]. One can see that $\Delta K \sim 20$ for transitions between different configurations, and $\Delta K \sim 1$ for transitions within one configuration. For example, for two clock transitions of Os^{16+} ($^3H_6$ - $^3F_4$ and $^3F_4$ - $^3F_4^o$),

$$\frac{\delta\omega_a}{\omega_a} - \frac{\delta\omega_b}{\omega_b} \approx 25\frac{\delta\alpha}{\alpha}. \tag{13}$$

Note that it looks beneficial to search for transitions with small ω for the sake of having a large enhancement factor ($K = 2q/\omega$). However, sometimes such transitions have no advantage since the accuracy of the measurements is equally important and the ratio of the relative experimental uncertainty to the relative change of ω due to variation of α often does not depend on ω [$(\delta\omega_{\mathrm{expt}}/\omega)/(\delta\omega_\alpha/\omega) = \delta\omega_{\mathrm{expt}}/\delta\omega_\alpha$]—see Ref. [25] for a detailed discussion. Large values of q in HCIs give a real advantage.

B. Einstein equivalence principle violation

Local position invariance (LPI), local Lorentz invariance (LLI), and the weak equivalence principle form the Einstein

TABLE VII. Parameters of the Os^{16+} and Ir^{17+} ions relevant to the search for the variation of α. The values of the q coefficients for the Ir^{17+} ion are taken from Ref. [5]. The enhancement factor K is given by $K = 2q/E$.

State		E (cm^{-1})	q (cm^{-1})	K
		Os^{16+}, even states		
$4f^{12}5s^2$	$^3H_6$	0	0	0
	$^3F_4$	9583	−1427	−0.30
	$^3H_5$	22433	19401	1.73
	$^1G_4$	30643	20900	1.36
	$^3F_2$	30675	6870	0.45
	$^3F_3$	33525	19300	1.15
		Os^{16+}, odd states		
$4f^{13}5s$	$^3F^o_4$	32908	337726	23.9
	$^3F^o_3$	37432	339746	20.8
		Ir^{17+}, odd states		
$4f^{13}5s$	$^3F^o_4$	0	0	0
	$^3F^o_3$	4647	2065	0.9
	$^3F^o_2$	25198	24183	1.9
	$^1F^o_3$	30167	25052	1.7
		Ir^{17+}, even states		
$4f^{12}5s^2$	$^3H_6$	29695	−385367	−26
	$^3F_4$	39563	−387086	−20
	$^3H_5$	53668	−362127	−13
	$^3F_2$	62140	−378554	−12
	$^1G_4$	62380	−360678	−12
	$^3F_3$	65438	−362313	−11
	$^3H_4$	84662	−339253	−8
	$^1D_2$	91341	−363983	−8
	$^1J_6$	103487	−364732	−7

equivalence principle, which is the foundation of general relativity. Some extensions of the standard model allow for violation of these invariances. The LPI violating term can be written as (see, e.g., Ref. [35] and references therein)

$$\hat{H}_{\rm LPI} = C_{00}\frac{2}{3}\frac{U}{c^2}\hat{K}, \tag{14}$$

where C_{00} is an unknown constant, U is the gravitation potential, c is the speed of light, and $\hat{K}$ is the operator of the kinetic energy, which in the relativistic case can be written as $\hat{K} = c\gamma_0\gamma^i p_i/2$, $\mathbf{p} = -i\hbar\nabla$ is the operator of electron momentum.

The presence of term (14) in the Hamiltonian causes the change of the atomic frequencies due to the change of the gravitation potential U (e.g., due to the annual variation of the Sun-Earth distance). It can be shown using the virial theorem that in the nonrelativistic limit all atomic frequencies change at the same rate and the effect is not detectable [36]. Therefore, it is convenient to describe the effect in terms of the so-called relativistic factor R, which indicates the deviation from the nonrelativistic virial theorem in the relativistic case [36],

$$R_{ab} = -\frac{E_{Ka} - E_{Kb}}{E_a - E_b}, \tag{15}$$

where E_{Ka} is the kinetic part of the energy of the atomic state a and E_a is its full energy. Then the relative change of two atomic frequencies can be written as

$$\frac{\Delta\omega_{ab}}{\omega_{ab}} - \frac{\Delta\omega_{cd}}{\omega_{cd}} = -(R_{ab} - R_{cd})\frac{2}{3}c_{00}\frac{\Delta U}{c^2}. \tag{16}$$

The highest sensitivity of atomic frequencies to the variation of the gravitation potential U can be achieved for transitions between states with very different values of the relativistic factor R. It turns out that, similar to the case of variation of α, the highest sensitivity is for the transitions between states of different configurations.

To calculate the values of R, one needs to calculate kinetic energies E_K caused by the kinetic energy operator $\hat{K}$. In principle, one can use the standard approach based on the RPA equations (5) and calculating matrix elements (6). However, calculations of the matrix elements of the kinetic energy operator are very sensitive to the correlation effects and one needs to include many minor contributions for stable results. It is more practical to use the so-called finite-field approach in which the calculation of the energy shift caused by a scalar operator is reduced to the calculation of the energy. The operator is added to the Dirac equations with a rescaling parameter s, calculations are repeated several times for different but small values of s and then extrapolated to $s = 1$. In our case, the Dirac equations with a rescaled operator of kinetic energy can be written as

$$\left(\frac{\partial f}{\partial r} + \frac{\kappa}{r}f\right)(1+s) - [1 + \alpha^2(\epsilon - \hat{V})]g = 0,$$
$$\left(\frac{\partial g}{\partial r} - \frac{\kappa}{r}g\right)(1+s) + (\epsilon - \hat{V})f = 0. \tag{17}$$

We perform calculations for several values of s from $s = 0$ to $s = 10^{-5}$, extrapolate the results to $s = 1$ to get the kinetic energies E_K, and use Eq. (15) to get the values of R. The results for the Os^{16+} and Ir^{17+} ions are presented in Table VIII. Calculations show that the energy shift caused by the kinetic energy operator $\hat{K}$ is similar for all states of the same configuration. Different values of R are mostly due to different energy intervals in the denominator of Eq. (15). The values of ΔR are presented with respect to the ground state. Therefore, the values are relatively small for all states of the ground-state configuration. On the other hand, the values of ΔR are large for the transitions between states of different configurations. Here $R \gg 1$, which is probably common for all HCI. In contrast, $R \sim 1$ for neutral atoms [27]. Note also that ΔR for transitions between states of different configurations of Os^{16+} and Ir^{17+} ions have different signs. This is because of the different order of states in the two ions.

The LLI violating term can be written as

$$\hat{H}_{\rm LLI} = -\tfrac{1}{6}C_0^{(2)}T_0^{(2)}, \tag{18}$$

where $T_0^{(2)}$ is a tensor operator $T_0^{(2)} = c\gamma_0(\gamma^j p_j - 3\gamma^3 p_3)$. The presence of term (18) in the Hamiltonian leads to the

TABLE VIII. Parameters of the Os^{16+} and Ir^{17+} ions relevant to the search for the Einstein equivalence principle violation. The values of the relativistic factors R are presented with respect to the ground state ($\Delta R_{ag} = R_a - R_g$).

State		E (cm^{-1})	ΔR	$\langle v\|\|T^{(2)}\|\|v\rangle$ (a.u.)
		Os^{16+}, even states		
$4f^{12}5s^2$	$^3H_6$	0	0	−299
	$^3F_4$	9583	0.2	24
	$^3H_5$	22433	7	−256
	$^1G_4$	30643	5	−106
	$^3F_2$	30675	2	122
	$^3F_3$	33525	5	68
		Os^{16+}, odd states		
$4f^{13}5s$	$^3F^o_4$	32908	18	−272
	$^3F^o_3$	37432	17	−223
		Ir^{17+}, odd states		
$4f^{13}5s$	$^3F^o_4$	0	0	−283
	$^3F^o_3$	4647	3	−233
	$^3F^o_2$	25198	3	−197
	$^1F^o_3$	30167	3	−254
		Ir^{17+}, even states		
$4f^{12}5s^2$	$^3H_6$	29695	−30	−311
	$^3F_4$	39563	−20	26
	$^3H_5$	53668	−13	−266
	$^3F_2$	62140	−11	131
	$^1G_4$	62380	−11	−107
	$^3F_3$	65438	−10	71
	$^3H_4$	84662	−7	−138
	$^1D_2$	91341	−7	95
	$^1J_6$	103487	−5	−612

dependence of atomic frequencies on the orientation of the apparatus in space. For the interpretation of the measurements, one needs to know the values of the reduced matrix elements of the operator $T_0^{(2)}$. We perform the calculations for the Os^{16+} and Ir^{17+} ions using the standard approach described in Sec. II B. The results are presented in Table VIII.

It was stated in Refs. [22,23] that to study the LLI violation one could measure the frequency of the transitions between states with different values of the projection of the total electron momentum J_z within one metastable state. A large value of the matrix element of the $T_0^{(2)}$ operator and a long lifetime of the state are needed for high sensitivity. In Os^{16+} and Ir^{17+} we have large values of the matrix element in many states, including the ground state. In both ions the values are larger than those in the Yb^+ ion suggested for the most sensitive measurements in Ref. [23]. This makes the ions attractive candidates for the study of the LLI violation.

C. Search for new bosons using nonlinearities of the King plot

It was suggested in Refs. [18,19] that nonlinearities of the King plot can be used to put limits on new interactions. The isotope shift ν for a specific atomic transition a can be written in the simplest form as

$$\nu_a = F_a \delta\langle r^2\rangle_{ij} + K_a \mu_{ij}. \tag{19}$$

Here F_a is the field shift constant, K_a is the mass shift constant, $\delta\langle r^2\rangle_{ij}$ is the change of the root-mean-square nuclear radius between isotopes i and j, and $\mu_{ij} = 1/m_i - 1/m_j$ is the reduced mass of the two isotopes. Here we neglect the higher-order in nuclear structure terms (e.g., terms $\sim\delta\langle r^2\rangle_{ij}^2$, $\delta\langle r^4\rangle_{ij}$, etc.). If we have two transitions, then finding $\delta\langle r^2\rangle_{ij}$ from Eq. (19) and substituting it into a similar equation for another transition leads to

$$\tilde{\nu}_{aij} = \frac{F_a}{F_b}\tilde{\nu}_{bij} - \frac{F_a}{F_b}K_b + K_a, \tag{20}$$

where $\tilde{\nu} = \nu/\mu$. This equation presents a straight line on the $(\tilde{\nu}_a, \tilde{\nu}_b)$ plane (the King plot). At least two transitions and four isotopes are needed to see deviations from the straight line. These conditions are satisfied for the Os^{16+} ion. Extra terms in Eq. (19) can lead to nonlinearities of the King plot. For example, if we have extra electron-neutron interaction mediated by a scalar boson of mass m_ϕ via a Yukawa-type interaction, then there is a contribution to the isotope shift due to different number of neutrons in two isotopes. The corresponding extra term can be written as $\frac{\alpha_{NP}}{\alpha}\Delta N_{ij} D_a$, where α_{NP} is a dimensionless constant of the strength of the new interaction, α is the fine-structure constant, ΔN_{ij} is the difference in the number of neutrons in isotopes i and j, and $D = \langle \exp(-m_\phi c r/\hbar)/r\rangle$. Then Eq. (20) becomes

$$\tilde{\nu}_{aij} = \frac{F_a}{F_b}\tilde{\nu}_{bij} - \frac{F_a}{F_b}K_b + K_a + D_b\gamma_{ij}\left(\frac{F_a}{F_b} - \frac{D_a}{D_b}\right). \tag{21}$$

Here $\gamma_{ij} = \frac{\alpha_{NP}}{\alpha}\Delta N/\mu_{ij}$. The last term in Eq. (21) depends on the isotopes and, therefore, may break the linearity of the King plot. Studying possible nonlinearities puts limit on the value of α_{NP} if the values of F and D are known. We calculate these values for different states of Os^{16+} using the technique described in Sec. II B. The results are presented in Table IX. The value of D depends on the mass of the extra boson m_ϕ.

TABLE IX. Field shift constants F and energy shifts D due to the Yukawa-type electron-nucleon interaction. D_1 is calculated at $m_\phi = 3$ MeV, and D_2 is calculated at $m_\phi = 0.3$ MeV. All values are given with respect to the ground state.

State		E (cm^{-1})	F (MHz/fm^2)	D_1 (GHz)	D_2 (GHz)
		Even states			
$4f^{12}5s^2$	$^3H_6$	0	0	0	0
	$^3F_4$	9583	93	−0.010	−0.177
	$^3H_5$	22433	−1487	0.157	2.86
	$^1G_4$	30643	−1612		
	$^3F_2$	30675	−564	0.047	0.879
	$^3F_3$	33525	−1487	0.157	2.86
		Odd states			
$4f^{13}5s$	$^3F^o_4$	32908	5.32[+5]	−52.3	−490
	$^3F^o_3$	37432	5.32[+5]	−52.3	−490

For mass $m_\phi > 30$ MeV, the radius of the new interaction $\hbar/m_\phi c$ is smaller than the nuclear radius $R_N = 6.5$ fm and the new interaction is indistinguishable from the field shift. In this case $D_a/D_b = F_a/F_b$ and the last term in Eq. (20) vanishes. We calculate D for two values of m_ϕ, 3 and 0.3 MeV, which correspond to the new interaction radii $r = 10R_N$ and $r = 100R_N$. For these values of D the last term in Eq. (20) is not zero and can be used to put limits on $\alpha_{\rm NP}$ at given m_ϕ.

Note that higher-order nuclear structure terms can also lead to the nonlinearities of the King plot. For example, it was demonstrated in Ref. [21] that observed nonlinearities of the King plot in Yb^+ can be explained by significant variation of the nuclear deformation between Yb isotopes (which produces terms $\sim\delta\langle r^4\rangle$). Unfortunately, these higher-order terms cannot be calculated with the accuracy exceeding the accuracy of the measurements of the King plot nonlinearity in Yb^+. As a result, the limits on the new interaction have been obtained under the assumption that this new interaction is the only source of nonlinearities. Therefore, we do not consider higher-order terms in this work since their calculations are unreliable and they will be neglected anyway. However, corresponding nonlinearities are likely to be smaller for Os than those for Yb. This is because nuclear calculations suggest that the nuclear deformation for all stable even isotopes of Os are about the same (see Table I and Ref. [17]). Equal values of the nuclear quadrupole deformation β produce equal energy shifts and no nonlinearities [21].

V. CONCLUSION

We have studied in detail the electronic structure of the Ir^{17+} and Os^{16+} ions using advanced theoretical techniques. Good agreement with available experimental data and earlier most advanced calculations is achieved. Calculations reveal many useful features of both ions relevant to their use for very accurate optical clocks sensitive to new physics. The Os^{16+} ion has at least three long-living states and three transitions which are good candidates for clock transitions. One of the transitions is very sensitive to the variation of the fine-structure constant. Many states of the ion, including the ground state, are sensitive to the local Lorentz invariance and local position invariance violation. The latter feature is likely to be common for all HCIs with open $4f$ or $5f$ shells. In addition, the Os^{16+} ion can be used to study new electron-neutron interactions using the King plot and its possible nonlinearities.

ACKNOWLEDGMENTS

The authors are grateful to Hendrik Bekker for careful reading of the manuscript and many useful comments. This work was supported by the Australian Research Council under Grants No. DP230101058 and No. DP200100150.

[1] J. C. Berengut, V. A. Dzuba, and V. V. Flambaum, Enhanced laboratory sensitivity to variation of the fine-structure constant using highly charged ions, Phys. Rev. Lett. **105**, 120801 (2010).

[2] V. V. Flambaum and S. G. Porsev, Enhanced sensitivity to the fine-structure constant variation in Th IV atomic clock transition, Phys. Rev. A **80**, 064502 (2009).

[3] H. Bekker, A. Borschevsky, Z. Harman, C. H. Keitel, T. Pfeifer, P. O. Schmidt, J. R. Crespo López-Urrutia, and J. C. Berengut, Detection of the $5p - 4f$ orbital crossing and its optical clock transition in Pr^{9+}, Nat. Commun. **10**, 5651 (2019).

[4] J. C. Berengut, V. A. Dzuba, V. V. Flambaum, and A. Ong, Highly charged ions with $E1$, $M1$, and $E2$ transitions within laser range, Phys. Rev. A **86**, 022517 (2012).

[5] J. C. Berengut, V. A. Dzuba, V. V. Flambaum, and A. Ong, Electron-hole transitions in multiply charged ions for precision laser spectroscopy and searching for variations in α, Phys. Rev. Lett. **106**, 210802 (2011).

[6] J. C. Berengut, V. A. Dzuba, V. V. Flambaum, and A. Ong, Optical transitions in highly charged californium ions with high sensitivity to variation of the fine-structure constant, Phys. Rev. Lett. **109**, 070802 (2012).

[7] V. A. Dzuba, A. Derevianko, and V. V. Flambaum, Ion clock and search for the variation of the fine-structure constant using optical transitions in Nd^{13+} and Sm^{15+}, Phys. Rev. A **86**, 054502 (2012).

[8] M. G. Kozlov, M. S. Safronova, J. R. Crespo López-Urrutia, and P. O. Schmidt, Highly charged ions: Optical clocks and applications in fundamental physics, Rev. Mod. Phys. **90**, 045005 (2018).

[9] Y.-M. Yu, B. K. Sahoo, and B.-B. Suo, Highly charged ion (HCI) clocks: Frontier candidates for testing variation of fine-structure constant, Front. Phys. **11**, 1104848 (2023).

[10] V. A. Dzuba, V. V. Flambaum, and H. Katori, Optical clock sensitive to variation of the fine-structure constant based on the Ho^{14+} ion, Phys. Rev. A **91**, 022119 (2015).

[11] T. Nakajima, K. Okada, M. Wada, V. A. Dzuba, M. S. Safronova, U. I. Safronova, N. Ohmae, H. Katori, and N. Nakamura, Visible spectra of highly charged holmium ions observed with a compact electron beam ion trap, Nucl. Instrum. Methods Phys. Res. Sect. B **408**, 118 (2017).

[12] A. Windberger, J.R. Crespo López-Urrutia, H. Bekker, N.S. Oreshkina, J.C. Berengut, V. Bock, A. Borschevsky, V.A. Dzuba, E. Eliav, Z. Harman, U. Kaldor, S. Kaul, U.I. Safronova, V.V. Flambaum, C.H. Keitel, P.O. Schmidt, J. Ullrich, and O.O. Versolato, Identification of optical transitions in complex highly charged ions for applications in metrology and tests of fundamental constants, Phys. Rev. Lett. **114**, 150801 (2015).

[13] A. Arvanitaki, J. Huang, and K. Van Tilburg, Searching for dilaton dark matter with atomic clocks, Phys. Rev. D **91**, 015015 (2015).

[14] Y. V. Stadnik and V. V. Flambaum, Can dark matter induce cosmological evolution of the fundamental constants of Nature? Phys. Rev. Lett. **115**, 201301 (2015).

[15] Y. V. Stadnik and V. V. Flambaum, Improved limits on interactions of low-mass spin-0 dark matter from atomic clock spectroscopy, Phys. Rev. A **94**, 022111, (2016).

[16] C. Cheung, M. S. Safronova, S. G. Porsev, M. G. Kozlov, I. I. Tupitsyn, and A. I. Bondarev, Accurate prediction of clock

transitions in a highly charged ion with complex electronic structure, Phys. Rev. Lett. **124**, 163001 (2020).

[17] S. E. Agbemava, A. V. Afanasjev, D. Ray, and P. Ring, Global performance of covariant energy density functionals: Ground state observables of even-even nuclei and the estimate of theoretical uncertainties, Phys. Rev. C **89**, 054320 (2014).

[18] C. Delaunay, R. Ozeri, G. Perez, and Y. Soreq, Probing atomic Higgs-like forces at the precision frontier, Phys. Rev. D **96**, 093001 (2017).

[19] J. C. Berengut, D. Budker, C. Delaunay, V. V. Flambaum, C. Frugiuele, E. Fuchs, C. Grojean, R. Harnik, R. Ozeri, G. Perez, and Y. Soreq, Probing new long-range interactions by isotope shift spectroscopy, Phys. Rev. Lett. **120**, 091801 (2018).

[20] S. O. Allehabi, V. A. Dzuba, V. V. Flambaum, A. V. Afanasjev, and S. E. Agbemava, Using isotope shift for testing nuclear theory: The case of nobelium isotopes, Phys. Rev. C **102**, 024326 (2020).

[21] S. O. Allehabi, V. A. Dzuba, V. V. Flambaum, and A. V. Afanasjev, Nuclear deformation as a source of the nonlinearity of the King plot in the Yb+ ion, Phys. Rev. A **103**, L030801 (2021).

[22] R. Shaniv, R. Ozeri, M. S. Safronova, S. G. Porsev, V. A. Dzuba, V. V. Flambaum, and H. Häffner, New methods for testing Lorentz invariance with atomic systems, Phys. Rev. Lett. **120**, 103202 (2018).

[23] V. A. Dzuba, V. V. Flambaum, M. S. Safronova, S. G. Porsev, T. Pruttivarasin, M. A. Hohensee, and H. Häffner, Strongly enhanced effects of Lorentz symmetry violation in entangled Yb^+ ions, Nat. Phys. **12**, 465 (2016).

[24] V. A. Dzuba, J. C. Berengut, C. Harabati, and V. V. Flambaum, Combining configuration interaction with perturbation theory for atoms with a large number of valence electrons, Phys. Rev. A **95**, 012503 (2017).

[25] V. A. Dzuba, V. V. Flambaum, and S. Schiller, Testing physics beyond the standard model through additional clock transitions in neutral ytterbium, Phys. Rev. A **98**, 022501 (2018).

[26] B. G. C. Lackenby, V. A. Dzuba, and V. V. Flambaum, Calculation of atomic spectra and transition amplitudes for the superheavy element Db ($Z = 105$), Phys. Rev. A **98**, 022518 (2018).

[27] V. A. Dzuba, S. O. Allehabi, V. V. Flambaum, J. Li, and S. Schiller, Time keeping and searching for new physics using metastable states of Cu, Ag, and Au, Phys. Rev. A **103**, 022822 (2021).

[28] V. A. Dzuba, V. V. Flambaum, and M. S. Safronova, Breit interaction and parity non-conservation in many-electron atoms, Phys. Rev. A **73**, 022112 (2006).

[29] I. Lindgren, H. Persson, S. Salomonson, and L. Labzowsky, Full QED calculations of two-photon exchange for heliumlike systems: Analysis in the Coulomb and Feynman gauges, Phys. Rev. A **51**, 1167 (1995).

[30] V. V. Flambaum and J. S. M. Ginges, Radiative potential and calculations of QED radiative corrections to energy levels and electromagnetic amplitudes in many-electron atoms, Phys. Rev. A **72**, 052115 (2005).

[31] W. R. Johnson and J. Sapirstein, Computation of second-order many-body corrections in relativistic atomic systems, Phys. Rev. Lett. **57**, 1126 (1986).

[32] V. A. Dzuba, V. V. Flambaum, P. G. Silvestrov, and O. P. Sushkov, Correlation potential method for the calculation of energy levels, hyperfine structure and $E1$ transition amplitudes in atoms with one unpaired electron, J. Phys. B: At. Mol. Phys. **20**, 1399 (1987).

[33] V. Dzuba, Calculation of polarizabilities for atoms with open shells, Symmetry **12**, 1950 (2020).

[34] S. G. Porsev and A. Derevianko, Multipolar theory of blackbody radiation shift of atomic energy levels and its implications for optical lattice clocks, Phys. Rev. A **74**, 020502(R) (2006); **86**, 029904(E) (2012).

[35] T. Pruttivarasin, M. Ramm, S. G. Porsev, I. I. Tupitsyn, M. S. Safronova, M. A. Hohensee, and H. Hffner, Nature (London) **517**, 592 (2015).

[36] V. A. Dzuba and V. V. Flambaum, Limits on gravitational Einstein equivalence principle violation from monitoring atomic clock frequencies during a year, Phys. Rev. D **95**, 015019 (2017).